HHS Public Access

Author manuscript

Cell Rep. Author manuscript; available in PMC 2021 August 12.

Published in final edited form as:

Cell Rep. 2021 July 13; 36(2): 109343. doi:10.1016/j.celrep.2021.109343.

Feedback control of PLK1 by Apolo1 ensures accurate chromosome segregation

Leilei Xu[1,2,8], **Mahboob Ali**[1,8], **Wenxiu Duan**[3,8], **Xiao Yuan**[1,4,*], **Fatima Garba**[2], **McKay Mullen**[1,2], **Binwen Sun**[5], **Ina Poser**[6], **Hequan Duan**[1,2,3], **Jianlin Lu**[1], **Ruijun Tian**[4], **Yushu Ge**[3], **Lingluo Chu**[1,2], **Weijun Pan**[7], **Dongmei Wang**[1], **Anthony Hyman**[6], **Hadiyah Green**[2], **Lin Li**[7], **Zhen Dou**[1,3,*], **Dan Liu**[3,*], **Xing Liu**[1,2,*], **Xuebiao Yao**[1,2,9,*]

[1]MOE Key Laboratory for Membraneless Organelles and Cellular Dynamics, University of Science & Technology of China, Hefei 230027, China

[2]Keck Center for Molecular Imaging, Morehouse School of Medicine, Atlanta, GA 30310, USA

[3]Anhui Key Laboratory for Chemical Biology, Hefei National Center for Physical Sciences at Microscale, Hefei 230027, China

[4]Department of Chemistry, Southern University of Science and Technology, Shenzhen 518055, China

[5]National Chromatographic Research and Analysis Center, Dalian 116023, China

[6]Max Planck Institute for Molecular Cell Biology and Genetics, Pfotenhauerstrasse 108, 01307 Dresden, Germany

[7]Shanghai Institute of Biochemistry and Cell Biology, Chinese Academy of Sciences, Shanghai 200031, China

[8]These authors contributed equally

[9]Lead contact

SUMMARY

Stable transmission of genetic material during cell division requires accurate chromosome segregation. PLK1 dynamics at kinetochores control establishment of correct kinetochore-microtubule attachments and subsequent silencing of the spindle checkpoint. However, the

*Correspondence: yuanxiao@ustc.edu.cn (X.Y.), douzhen@ustc.edu.cn (Z.D.), dliu919@ustc.edu.cn (D.L.), xing1017@ustc.edu.cn (X.L.), yaoxb@ustc.edu.cn (X.Y.).

AUTHOR CONTRIBUTIONS

L.X. and X. Yao conceived the project. L.X. and M.A. designed and performed most biochemical experiments, cell biological characterization, and data analyses. X. Yuan and R.T. performed *in vitro* phosphorylation site identification and B.S. performed *in vivo* Apolo1 binding protein identification using mass spectrometric analyses. L.X., Y.G., L.C., and W.D. performed the FRET sensor assay, and D.L. constructed the PLK1 sensor. M.M. and F.G. conducted immunofluorescence analyses. A.H., I.P., Z.D., H.D., J.L., W.P., D.W., L.L., and H.G. contributed reagents. L.X., M.A., X. Yuan, Z.D., D.L., X.L., and X. Yao wrote the manuscript, and all authors have read and approved the manuscript.

SUPPLEMENTAL INFORMATION

Supplemental information can be found online at https://doi.org/10.1016/j.celrep.2021.109343.

DECLARATION OF INTERESTS

The authors declare no competing interests.

regulatory mechanism responsible for PLK1 activity in prometaphase has not yet been affirmatively identified. Here we identify Apolo1, which tunes PLK1 activity for accurate kinetochore-microtubule attachments. Apolo1 localizes to kinetochores during early mitosis, and suppression of Apolo1 results in misaligned chromosomes. Using the fluorescence resonance energy transfer (FRET)-based PLK1 activity reporter, we found that Apolo1 sustains PLK1 kinase activity at kinetochores for accurate attachment during prometaphase. Apolo1 is a cognate substrate of PLK1, and the phosphorylation enables PP1γ to inactivate PLK1 by dephosphorylation. Mechanistically, Apolo1 constitutes a bridge between kinase and phosphatase, which governs PLK1 activity in prometaphase. These findings define a previously uncharacterized feedback loop by which Apolo1 provides fine-tuning for PLK1 to guide chromosome segregation in mitosis.

Graphical abstract

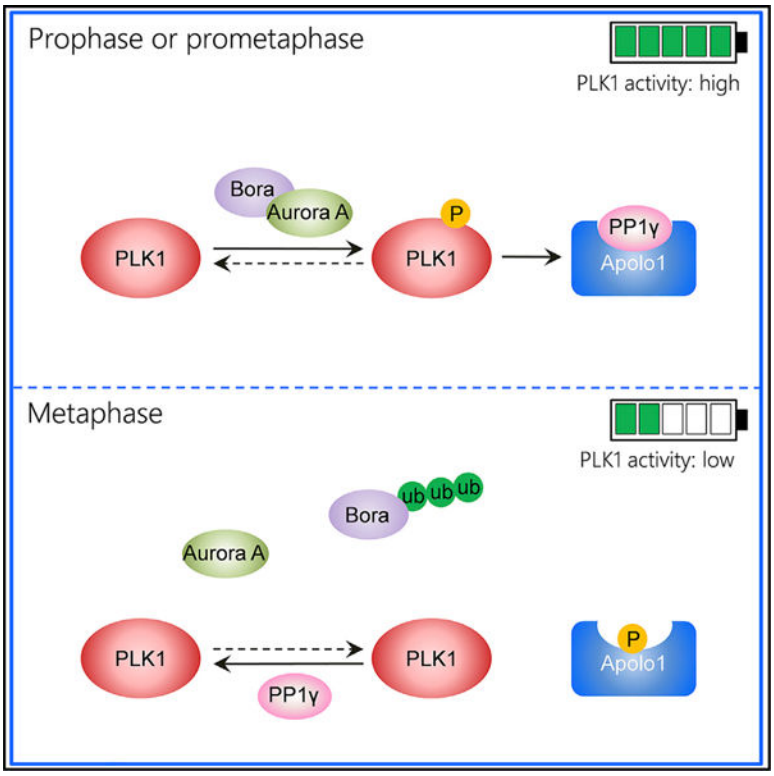

In brief

Xu et al. identify Apolo1, which governs PLK1 activity and promotes faithful chromosome segregation in prometaphase by bridging kinase and phosphatase activities.

INTRODUCTION

Faithful segregation of mitotic chromosomes requires proper bipolar attachment of sister chromatids to microtubules emanating from opposite spindle poles. It is the kinetochore that not only binds to spindle microtubules but also governs chromosome separation during

mitosis (Cleveland et al., 2003; Liu et al., 2020). In mitosis, several key mitotic kinases are responsible for regulating kinetochore-microtubule (kMT) attachments, including polo-like kinase 1 (PLK1) (Archambault and Glover, 2009; Zitouni et al., 2014). PLK1 is highly conserved among different species, with at least one PLK family member present from fungi to human (Archambault and Glover, 2009; Zitouni et al., 2014).

In vertebrate cells, PLK1 localizes to kinetochores during early mitosis and usually accumulates on unaligned chromosomes (Ahonen et al., 2005; Liu et al., 2012; Yu et al., 2020). During early mitosis, PLK1 stabilizes kMT attachments at kinetochores, whereas Aurora B destabilizes kMT attachments at kinetochores (Godek et al., 2015; Lampson and Kapoor, 2005). Therefore, a tug of war between PLK1 and Aurora B kinase establishes the balance of the initial formation of stable kMT attachments. Previous studies showed that Aurora B kinase activity was high during prophase (Lampson and Cheeseman, 2011; Liu et al., 2009); therefore, high PLK1 activity is needed to balance Aurora B activity for the initial establishment of stable kMT attachments. Prior work reported that Bora can facilitate Aurora A kinase to activate PLK1 kinase activity before mitotic entry, thus ensuring timely mitotic entry and cell-cycle progression (Macůrek et al., 2008; Seki et al., 2008b). In addition, it was reported that only a minimal amount of residual Aurora A-Bora complex could continue to sustain high PLK1 kinase activity during mitosis (Bruinsma et al., 2014). However, it is difficult to draw this conclusion, because (1) Bora degrades quickly and dramatically after nuclear envelop breakdown (NEBD), with only minimal amounts of Bora remaining (Seki et al., 2008a); (2) Cep192 facilitates Aurora A to activate PLK1 in centrosomes, but not at kinetochores (Joukov et al., 2014); and (3) Mypt1-PP1β phosphatase concurrently antagonizes PLK1 kinase activity at kinetochores during early mitosis (Dumitru et al., 2017; Yamashiro et al., 2008). These combined facts suggest that other undefined regulatory mechanisms for maintaining high PLK1 activity during early mitosis must exist and remain to be characterized.

Genes with mitotic functions such as *CDKN1B*, *AURKA*, and *TPX2* have similar transcriptional expression profiles during the cell cycle, because they are all induced in G2/M (de Lichtenberg et al., 2005). Several early studies demonstrated that the patterns seen in genome-wide expression experiments can be interpreted as indications of the status of cellular processes (Stuart et al., 2003; van Dam et al., 2012). Whitfield et al. (2002) reported that 566 genes in the human transcriptome are induced in G2 or G2/M, and subsequent characterization of these genes led to the identification of their functions in mitosis (Wong and Fang, 2006). Coexpression of genes of known function with poorly characterized or novel genes may provide a reference of gaining leads to the functions of uncharacterized genes (van Dam et al., 2012). Thus, using genes with known functions in a coexpression analysis could help identify and prioritize novel candidate genes for experimental verification.

We attempted to identify regulators of PLK1 using gene coexpression analysis, and we unexpectedly identified a previously uncharacterized gene, *Apolo1*, as a novel PLK1 binder and uncovered its vital role in regulating PLK1 kinase activity. The associating protein with Polo1 (Apolo1) colocalizes with PLK1 to kinetochores during early mitosis, and suppression of Apolo1 results in aberrant mitosis. Mechanistically, Apolo1 binds to the

PLK1 PBD (polo-box domain) domain with its N terminus, whereas its C terminus contains a canonical PP1 docking motif. Importantly, the PP1 binding activity is regulated by PLK1 phosphorylation, which eliminates PP1γ binding. Altogether, our findings establish a novel PLK1-Apolo1-PP1γ feedback loop required for fine-tuning of PLK1 kinase activity during early mitosis.

RESULTS

Identification of a novel kinetochore protein, Apolo1, essential for mitosis

Genes with mitotic functions exhibit similar transcriptional expression profiles, because they are all induced in G2/M (de Lichtenberg et al., 2005). In tumor cells, known mitotic regulators are transcriptionally up- or downregulated in concert and project stereotypical covariation profiles (Rhodes et al., 2004). Through analysis of transcriptional array data from cancer tissue samples, several mitotic regulators, such as HURP and SKAP, were identified and characterized (Fang et al., 2009; Wong and Fang, 2006).

By evaluating the transcriptional array data reported by Segal et al. (2004) and van Dam et al. (2012), we categorized genes covaried with known mitotic regulators such as *PLK1* (Boyle et al., 2004). Our analyses generated a list of uncharacterized genes associated with PLK1 kinase in proliferating cells (Figure S1A; Table S1), in which *C1orf112* encodes an 853-amino acid protein of unknown function. Computational analyses show that *C1orf112* is evolutionarily conserved (Edogbanya et al., 2021). Nevertheless, *C1orf112* contains no characterized structural motifs (Figure 1A). Given its functional interaction with PLK1, identified in this study, we refer to the protein encoded by *C1orf112* as Apolo1.

To determine the protein level of Apolo1 relative to PLK1 in mitosis, aliquots of synchronized HeLa cells in G1/S and in mitosis were collected for western blotting. As shown in Figure 1B, the level of Cyclin B exhibited an estimated 10-fold increase during mitosis. In the same preparation, the level of Apolo1 was elevated approximately 5-fold, similar to that of PLK1 (Figure 1B). The covariation profiles between PLK1 and Apolo1 prompted us to examine their respective patterns of sub-cellular distribution using immunofluorescent staining. As shown in Figure 1C, Apolo1 exhibits light deposition in the nucleus of interphase cells when PLK1 is absent from the nucleus (first panel, a; asterisk). Interestingly, both Apolo1 and PLK1 were found on chromosome structures in the neighboring prometaphase cells (a and a′; arrows). Using anti-centromere antibody (ACA) as a reference, we found that Apolo1 and PLK1 are apparently colocalized to the centromeres in a nearby prometaphase cell (Figure 1C, second panel, b and b′; white arrows). Careful examination of Apolo1 localization revealed its colocalization with PLK1 to the kinetochore of prometaphase cells (Figure 1C, second panel, b”; arrowheads). A magnified image shows that the localization of Apolo1 is superimposed with a subset of PLK1 signals at the kinetochore, validating their spatiotemporal relationship in mitosis (Figure 1C, second panel, b”, arrows). Most of Apolo1 is liberated from the centromeres, while PLK1 is also released from the centromere during metaphase alignment (Figure 1C, second panel, b and b′; yellow arrows), which is consistent with the distribution dynamics of PLK1 in the literature (Liu et al., 2012; Zhang et al., 2011). Both Apolo1 and PLK1 relocate to the central spindle in anaphase and to the midbody in telophase cells (Figure 1C,

c and d; arrows), demonstrating the similar spatiotemporal dynamics of Apolo1 and PLK1 distribution during mitosis.

Because Apolo1 localizes to the kinetochores and exhibits cell-cycle-dependent distribution during mitosis, we next determined whether suppression of Apolo1 would generate mitotic defects using time-lapse microscopy. As shown in Figure 1D, cells treated with scramble small interfering RNA (siRNA) progressed normally through mitosis; however, Apolo1-suppressed cells exhibited a high frequency of chromosome segregation defects, including chromosome misalignment and chromosome bridges (arrowheads). Our statistical analyses from three independent experiments demonstrate that suppression of Apolo1 resulted in chromosome segregation error, because most exhibited misalignment (Figure 1E) ($p < 0.001$, $n = 50$), suggesting that Apolo1 is essential for accurate chromosome progression. Thus, we conclude that Apolo1 is a novel kinetochore protein essential for accurate mitosis.

Apolo1 ensures accurate PLK1 kinase activity during early mitosis

The kinetochore localization and requirement of Apolo1 for accurate chromosome segregation prompted us to examine the functional interactions of Apolo1-PLK1 in mitosis. To evaluate the interaction of PLK1 with Apolo1 and identify proteins bound to Apolo1 in early mitosis, we used the anti-FLAG affinity to isolate the FLAG-Apolo1 complex from mitotic HeLa cells in parallel for mass spectrometry analyses (Figure S1B). Several mitotic components, such as PLK1, Mypt1, Cdk1, Misp, and PP1, are repeatedly found in the Apolo1 complex (Figure S4A; Table S2), supporting our coexpression analyses that Apolo1 and PLK1 form a functional complex in mitotic cells.

To assess the impact of Apolo1 deficiency on PLK1 activity, we introduced two siRNA oligonucleotide duplexes to Apolo1 by transfection into HeLa cells and carried out western blotting analyses using phosphorylated PLK1 (pT210-PLK1) as the readout (Liu et al., 2012; Yu et al., 2020). As shown in Figures S1C and S1D, western blotting with anti-Apolo1 antibody and quantitative analysis revealed that the two independent siRNA oligonucleotides caused remarkable suppression of Apolo1 protein levels at 48 h. This suppression was specific, because it did not alter the levels of other proteins, such as tubulin, PLK1, and Aurora B (Figure 2A). Statistical analyses show that suppression of Apolo1 significantly reduced PLK1 kinase activity, as judged by relative pT210-PLK1 level (Figure 2B) ($p < 0.001$). To examine whether suppression of Apolo1 affects PLK1 activity at the kinetochore, we carried out triple immunofluorescence analyses in which the protein level and related kinase activity of PLK1 were assessed in centromere-marked HeLa cells. In control cultures transfected with scramble siRNA, PLK1 and pT210-PLK1 were colocalized to the prometaphase kinetochores annotated by ACA (Figure 2C, top panels). In addition, centrosomal localization of pT210-PLK1 was readily apparent (Figure 2C, top panels; asterisks). In Apolo1-depleted cells, the levels of kinetochore-bound PLK1 protein appeared unchanged (Figure 2C, a′). However, the kinase activity of PLK1, as judged by the level of pT210-PLK1, has been minimized in Apolo1-depleted cells (Figure 2C, b′). Quantitation of normalized pixel intensities showed that when the Apolo1 protein level was suppressed by siApolo1, pT210-PLK1 levels were significantly reduced (Figure 2D) ($p < 0.01$), indicating that Apolo1 is required to efficiently maintain PLK1 activity at the kinetochore. To avoid the

potential off-target effect, we employed another siRNA targeted to 3′ UTR (3′ untranslated region) of Apolo1, which also showed high efficiency in suppression of Apolo1 protein expression (Figure S1E). Quantitation of normalized pixel intensities showed that when the Apolo1 protein level was suppressed by siApolo1-UTR, pT210-PLK1 levels were significantly reduced to a level comparable to that of siApolo1–2# (Figure 2D). These data suggest that Apolo1 is a positive regulator for PLK1 kinase activity during early mitosis. In our positive control experiment, suppression of Bora, a well-characterized PLK1 activator, resulted in dramatic reduction of kinetochore-associated pT210-PLK1 (Figure 2D) ($p < 0.001$), which is consistent with previous studies (Seki et al., 2008b). To directly visualize real-time PLK1 kinase activity change at the kinetochore when the Apolo1 protein level was reduced, we used the fluorescence resonance energy transfer (FRET)-based PLK1 kinase sensor tagged with Hec1 to probe PLK1 kinase activity at the kinetochores of mitotic chromosomes (Chu et al., 2012; Liu et al., 2012). Because 293T cells express Apolo1 mRNA higher than that of HeLa cells (Figure S1F) and are more easily undergo transfection, we selected 293T cells for quantitative measurement of PLK1 activity at the kinetochore. As reported in our early studies, FRET-based sensors report the quantitative change in PLK1 substrate phosphorylation at the kinetochore in living cells (Figure 2E). The change of FRET intensity is a function of PLK1 activity, because addition of BI2536, a chemical inhibitor of PLK1, abolished the FRET signal. Consistent with aforementioned results, mitotic 293T cells transfected with Apolo1 siRNA against 3′ UTR showed a significant reduction of PLK1 kinase activity compared with the control group (Figure 2E) (Lénárt et al., 2007). As shown in Figure 2F, our quantitative analyses demonstrate that suppression of Apolo1 significantly reduced PLK1 kinase activity in prometaphase cells, consistent with what was seen in chemical inhibition ($p < 0.05$; $n > 20$). To exclude the cell-line-specific activity detected earlier, we subsequently measured the FRET-based PLK1 activity in mitotic HeLa (Figure S1G) and U2OS cells (Figure S1H). The statistical analyses showed that depletion of Apolo1 reduced PLK1 kinase activity in HeLa and U2OS cells. Thus, we conclude that Apolo1 is important for PLK1 kinase activity in mitosis.

Apolo1 is required for maintaining, but not activating, PLK1 kinase activity

Previous work reported that PLK1 kinase activity is regulated by at least two distinct pathways: PLK1 is activated by the Aurora A-Bora complex and inactivated by the Mypt1-PP1β complex (Chiyoda et al., 2012; Dumitru et al., 2017; Seki et al., 2008b; Yamashiro et al., 2008). The finding that suppression of Apolo1 resulted in PLK1 kinase activity reduction suggests that Apolo1 positively regulates PLK1 kinase by either activating PLK1 or antagonizing a negative regulator of PLK1, such as PP1 phosphatase activity toward PLK1. Because the pT288-Aurora A level was apparently unaltered by Apolo1 depletion compared with the pT210-PLK1 level (Figure 2A, fourth panel, lanes 2 and 3), we carried out immunofluorescence analyses of both pT288-Aurora A and Aurora A in control and Apolo1-suppressed cells. As shown Figures S2A and S2B, suppression of Apolo1 did not apparently affect the level of pT288-Aurora A in prometaphase and metaphase HeLa cells, whereas Aurora A chemical inhibitor VX-680 apparently abolished the signal of pT288-Aurora A (bottom panel). Consistently, pT288-Aurora A or Aurora A signal intensity was not affected by Apolo1 suppression based on quantitative analyses (Figures S2C and

S2D). Thus, we conclude that regulation of PLK1 by Apolo1 is not related to T-loop phosphorylation of Aurora A.

To delineate the mechanism underlying Apolo1-elicited PLK1 kinase activity, we then carried out enzymatic assay and measured the kinetic parameters of recombinant PLK1 toward substrate Cep55 at constant level of ATP. As shown in Figure 3A, the maximal velocity of phosphorylation by PLK1 alone was slower compared with that of PLK1 preactivated by Aurora A plus Bora. These kinetics analyses indicate that phosphorylation of PLK1 by Aurora A in the presence of Bora achieved an optimal catalytic activity (Figure S2E). We next examined the impact of Apolo1 on PLK1 kinase activity. As shown in Figure 3A, the catalytic activity of PLK1 is not altered by addition of Apolo1 alone or Apolo1 plus Aurora A, suggesting that Apolo1 is unable to elicit conformational change of PLK1. Interestingly, addition of Apolo1 into PLK1 primed by Aurora A and Bora does not significantly increase the catalytic activity. Chemical inhibitor BI2536 abolished the PLK1 kinase activity elicited by Aurora A, Bora and Apolo1 (Figure S2E). Thus, we conclude that Apolo1 is required for maintaining PLK1 kinase activity, but not facilitating Aurora A to activate PLK1.

PLK1 interacts with Apolo1 both *in vivo* and *in vitro*

Because Apolo1 sustains PLK1 kinase activity *in vivo* and *in vitro*, we next sought to test whether Apolo1 could form a complex with PLK1 *in vivo*. As shown in Figure 3B, endogenous PLK1 immunoprecipitation brought down Apolo1 protein from mitotic cell lysates (lane 4). The reciprocal immunoprecipitation of endogenous Apolo1 confirmed that Apolo1 forms a complex with PLK1 kinase in mitotic cells (Figure S3A).

To determine the physical contacts and interfaces between Apolo1 and PLK1, we carried out immunoprecipitation using a series of deletion mutants of Apolo1 tagged with GFP (Figure 3C). As shown in Figure 3D, the N terminus of Apolo1 (Apolo1-N; 1–176 aa) binds to PLK1 (lane 4). Further pull-down assay using bacterially recombinant MBP (maltose binding protein)-PLK1 with glutathione S-transferase (GST)-Apolo1 truncations demonstrated that the N terminus (1–176 aa) of Apolo1 binds to PLK1 directly *in vitro* (Figure S3B). Thus, we conclude that Apolo1 physically interacts with PLK1 through its N-terminal region. We next sought to map the domain of PLK1, which binds with Apolo1 using a series of PLK1 deletion mutants, as illustrated in Figure 3E. As shown in Figures 3F and S3C, the PBD domain of PLK1 is the contact site for Apolo1 (lane 6). Thus, Apolo1 is a bona fide PLK1-regulating protein conserved in eukaryotic cells.

It is well established that PBD binds to phosphorylated peptides with the consensus sequence S-[pS/pT]-P/X (Elia et al., 2003). We found that the sequence from Ser42 to Gln44 in the N-terminal 176 amino acids of Apolo1 is consistent with the binding motif of the PBD domain. A previous study reported that Apolo1 is phosphorylated on Ser43, but the precise upstream kinase was not characterized (Zhou et al., 2013). We used the recombinant PLK1 kinase to phosphorylate the GST-Apolo1-N protein and subjected it to mass spectrometric analysis. Our analyses indicated that Ser43 of Apolo1 was phosphorylated by PLK1 in an *in vitro* phosphorylation assay (Figure S3D; Table S3). To further demonstrate whether Ser43 phosphorylation would affect PLK1-Apolo1 binding, we

carried out a coimmunoprecipitation assay with GFP-Apolo1 wild-type and Ser43 mutants, along with FLAG-PLK1-PBD. As shown in Figure S3E, the phosphorylation-mimicking mutant Apolo1 S43D exhibited significantly increased binding efficiency to PLK1 compared with that of Apolo1 wild type (WT), whereas the non-phosphorylatable mutant Apolo1 S43A exhibited decreased binding efficiency to PLK1 compared with that of Apolo1 WT. Thus, these data demonstrate that Apolo1 is a bona fide substrate of PLK1 and phosphorylation strengthens Apolo1-PLK1 interaction.

Apolo1 interacts with PP1γ directly via a canonical PP1 binding motif

Sequence alignments of Apolo1 among different vertebrate species were performed using the ClustalX algorithm, which identified a highly conserved KVVXF motif (Figure 4A). The KVVXF motif is a canonical PP1 docking motif (Hendrickx et al., 2009; Meiselbach et al., 2006), suggesting that Apolo1 may physically interact with PP1. Mass spectrometry analysis of FLAG-Apolo1 immunoprecipitates from mitotic cells indicated the presence of the catalytic subunit of PP1 (Figure S4A). To determine whether Apolo1 selectively binds to a particular PP1 isoform or isoforms, we carried out an immunoprecipitation assay in which Apolo1 was cotransfected with one of the three PP1 catalytic isoforms (α, β, and γ). As expected, Apolo1 formed a complex with the PP1 catalytic subunit *in vivo*; however, only isoform, PP1γ, exhibited binding to Apolo1 (Figure 4B, lane 8). To evaluate whether PP1γ physically interacts with Apolo1, a pull-down assay was carried out. As shown in Figure 4C, only the GST-PP1γ affinity matrix retains the recombinant MBP-Apolo1 protein *in vitro* (lane 5). The binding activity was further mapped to the C terminus of Apolo1 (Apolo1-C) *in vitro* (Figure S4B, lane 5). Therefore, these data indicate that Apolo1 is a bona fide interacting partner with PP1γ both *in vivo* and *in vitro*.

To evaluate whether the PP1 docking motif regulates Apolo1-PP1γ interaction, the characteristic PP1 docking motif KVVSF was mutated into AVAAA (the 4A mutant) and recombinant proteins were collected and used as the affinity matrix for a pull-down assay. As shown in Figure 4D, only the Apolo1 WT protein absorbed PP1γ, but the Apolo1 4A mutant did not (lanes 5 and 6). An immunoprecipitation assay of FLAG-PP1γ with hemagglutinin (HA)-Apolo1 WT and 4A mutant confirmed that the interaction of PP1γ with Apolo1 depends on the KVVSF motif (Figure S4C, lane 5). These data indicate that Apolo1 is a novel bona fide PP1γ-interacting protein via the classic docking motif KVVSF.

Because Apolo1 did not directly activate PLK1 activity in the kinase assay (Figure 3A), the hierarchy of interaction of Apolo1, PLK1, and PP1γ prompted us to examine whether PLK1 interacts with PP1γ in the absence of Apolo1. As shown in Figures S4D and S4E, immunoprecipitation of PLK1 from Apolo1-suppressed cells revealed that the association of PLK1 with Bora and PP1β was apparently unaffected, suggesting that Apolo1 did not participate in the Bora-PLK1 or PLK1-PP1β complex in mitotic cells.

Perturbation of the Apolo1-PP1γ interaction attenuates PLK1 kinase activity

Because Apolo1 binds to PP1γ and regulates PLK1 kinase activity, we sought to directly examine the PLK1 kinase activity *in vivo* in the absence of Apolo1-PP1γ interaction. As shown in Figure 4E, suppression of Apolo1 attenuated PLK1 activity in kinetochores of

mitotic 293T cells, as judged by the FRET-based sensor. This attenuation was rescued by exogenously expressed Apolo1 WT, but not the 4A mutant, as judged by statistical analyses (Figure 4F). Thus, these data indicate that the dynamic interaction between Apolo1 and PP1γ is important for orchestrating PLK1 kinase activity, because abrogation of Apolo1-PP1γ interaction significantly reduced PLK1 kinase activity at the kinetochore of mitotic cells.

We next examined phosphorylation of PLK1 activities using phospho-specific antibodies. First, we analyzed pT210-PLK1 in cells expressing Apolo1 WT and the Apolo1 4A mutant. Consistent with the earlier FRET sensor assay, western blotting analyses showed that disruption of Apolo1-PP1γ interaction led to a reduced level of pT210-PLK1 (Figure S4F, lane 4). Because Apolo1 WT and the 4A mutant remain localized to the kinetochore of prometaphase cells (Figure S4G), the inability of the Apolo1 mutant to rescue PLK1 activity mainly results from perturbation of the Apolo1-PLK1 interaction. We also performed the time-lapse imaging assay to assess the physiological effect of disrupting Apolo1-PP1γ binding in mitosis (Figure S4H). As expected, time-lapse imaging analyses of chromosome segregation in mitotic cells deficient in endogenous Apolo1 showed that Apolo1 WT, but not Apolo1 4A, had largely rescued mitotic defects such as lagging chromosomes (Figure 4G), chromosome misalignment (Figure 4H), and sister chromatid bridges in Apolo1-deficient cells (Figure 4I). Thus, these results indicate that Apolo1-PP1γ interaction plays an important role in orchestrating PLK1 kinase activity during mitosis.

PLK1-mediated phosphorylation of Ser744 abolished Apolo1 binding to PP1γ

Mounting evidence demonstrated that phosphorylation of the RV [S/T]F motifs is a general mechanism for negatively controlling the interaction of PP1 with its regulatory proteins (Nasa et al., 2018). Because Ser744 in the KVVSF motif among different vertebrate species was highly conserved, we sought to examine whether Ser744 is phosphorylated during mitosis. Computational analyses indicated that Ser744 is phosphorylated in highly proliferating tumor cells (Mertins et al., 2014, 2016). However, no specific upstream kinases were identified and characterized. Therefore, we next examined whether phosphorylation of Ser744 would affect its binding to PP1γ. We created phosphorylation-mimicking and non-phosphorylatable mutant Apolo1 S744D/A recombinant proteins and applied them as input to the GST-PP1γ affinity beads. As shown in Figure 5A, Apolo1 S744D was less efficient at binding PP1γ (lane 11), whereas Apolo1 S744A (lane 10) was retained on the GST-PP1γ affinity matrix, comparable with wild-type Apolo1 (lane 9). These data suggest that phosphorylation of Apolo1 at Ser744 regulates the interaction between Apolo1 and PP1γ.

To test whether PLK1 is responsible for Ser744 phosphorylation, we performed an *in vitro* kinase assay using PLK1. After the reaction, phosphorylated Apolo1 proteins were subjected to mass spectrometric analyses. As shown in Figure S5A, Ser744 is specifically phosphorylated by PLK1 (Table S4). To demonstrate that Ser744 is a cognate substrate for the PLK1 kinase, we performed an *in vitro* kinase assay using the PLK1 kinase to phosphorylate His-Apolo1-C WT and S744A in the presence of radioactive γ-ATP (^{32}P). As expected, PLK1 phosphorylated Apolo1-C WT, but not the S744A mutant (Figure 5B).

Thus, these data indicate that Ser744 is a cognate substrate for the PLK1 kinase during mitosis.

To examine the precise function of Ser744 phosphorylation in chromosome segregation during mitosis, we conducted real-time imaging analyses of chromosome segregation in cells expressing Apolo1 S744A/D mutants into HeLa cells deficient in endogenous Apolo1 protein. As shown in Figures S5B–S5D, expression of FLAG-Apolo1 WT and the S744A mutant largely rescued the mitotic defects seen in Apolo1-depleted cells ($p < 0.01$), whereas FLAG-Apolo1 S744D only partially rescued the mitotic defects, with lagging chromosomes or chromosome misalignments remaining. This suggests that PLK1-mediated Ser744 phosphorylation of Apolo1 negatively regulated its interaction with PP1γ, thus creating a negative feedback loop for maintaining proper PLK1 kinase activity during mitosis.

PLK1-Apolo1-PP1γ interaction constitutes a feedback loop for accurate PLK1 activity in mitosis

Consistent with previous studies (Chiyoda et al., 2012; Yamashiro et al., 2008), suppression of PP1γ and MYPT1 by siRNA treatment resulted in an increased level of pT210-PLK1 *in vivo*, indicating that PP1γ negatively regulates the kinase activity of PLK1 (Figure S5E). To delineate how Apolo1 functions in the PLK1-PP1γ signaling axis, we sought to perform an *in vitro* dephosphorylation assay using the active PLK1 kinase as the substrate. We first generated recombinant active PP1γ phosphatase and determined its phosphatase activity as previously reported (Dohadwala and Berndt, 1998; Zhang et al., 1992). As a first step of the trial experiment, aliquots of recombinant PP1γ phosphatase were incubated with pT210-PLK1 to determine an optimal time interval for the dephosphorylation reaction. As shown in Figure S5F, recombinant PP1γ dephosphorylated pT210-PLK1 in a time-dependent manner, as judged by the loss of phosphorylated Thr210. Statistical analyses from three independent preparations confirmed that PP1γ phosphatase is responsible for dephosphorylation of pT210-PLK1 (Figure S5G).

If Apolo1 sustains, but does not activate, PLK1 kinase activity, it is likely that Apolo1 may protect phosphorylated PLK1 kinase from dephosphorylation by PP1γ. To test this possibility, aliquots of phosphorylated PLK1 were incubated with different concentrations of PP1γ to determine the optimal concentration of phosphatase. As shown in Figure 5C, PP1γ removed phosphate from Thr210 of PLK1 in a dose-dependent manner. We next determine whether addition of Apolo1 modulates this dephosphorylation reaction. Specifically, aliquots of Apolo1 were mixed with PP1γ before incubation with pT210-PLK1 to initiate the dephosphorylation reaction. As shown in Figure 5D, dephosphorylation of PLK1, as judged by the level of pT210-PLK1, was attenuated by Apolo1 in a dose-dependent manner. Thus, these results define a novel regulatory mechanism in which Apolo1 protects PLK1 kinase activity by binding and sequestering PP1γ phosphatase activity.

DISCUSSION

Correct chromosome segregation ensures accurate mitotic progression, which depends on precise kMT attachment during early mitosis. Previous work revealed that PLK1 maintains

high kinase activity during prometaphase to balance Aurora B kinase activity, thus ensuring the initial establishment of kMT attachment during early mitosis (Foley and Kapoor, 2013; Liu et al., 2012). Because Bora degrades dramatically before mitotic entry (Seki et al., 2008a), how PLK1 kinase activity was maintained with high activity remains unclear. Here, our studies identified a new PLK1 regulator, Apolo1, which maintains PLK1 activity at the kinetochore in early mitosis. Apolo1 binds PP1γ via a canonical PP1 docking motif that sequesters phosphatase activity from PLK1. Apolo1 is subsequently phosphorylated at Ser744 by PLK1 during mitotic progression, which releases PP1γ for dephosphorylation of Thr210-PLK1. Thus, Apolo1 interactions with PLK1 and PP1γ constitute a novel feedback loop for precise spatiotemporal regulation of PLK1 activity in prometaphase (Figure 5E). In the future, it would be of great interest to see the binder of PP1γ after its liberation from the kinetochore.

Kinetochore kinases and phosphatases orchestrate control of chromosome segregation in mitosis (Liu et al., 2020). The functional PP1 holoenzyme consists of one catalytic subunit and one regulatory subunit (Meiselbach et al., 2006). PP1 regulatory proteins could function as PP1 activity regulators, substrate-targeting proteins, substrate adaptors, and/or substrates (Hendrickx et al., 2009). Previous studies defined the consensus motif for PP1 binding to be either in the relatively simple RVXF motif or in the more specified [H/K/R][0,1][V/I/L][^P][F/W] motif (Hendrickx et al., 2009; Meiselbach et al., 2006). Apolo1 binding to PP1γ through a KVVSF sequence conforms to the canonical PP1 binding motif, suggesting that Apolo1 is a novel PP1 regulatory protein. Apolo1 acts as a novel sequestering protein for PP1 by which Apolo1 blocks PP1γ access toward PLK1, which constitutes a novel mechanism of action underlying PLK1 activity control in mitosis.

Our studies reveal that phosphorylation of Ser744 by the PLK1 kinase within the KVVSF motif dramatically diminished Apolo1-PP1γ binding and that persistent phosphorylation failed to rescue the mitotic defects in Apolo1-deficient cells. Previous studies established the importance of the Aurora A-Bora complex in PLK1 activity control (Joukov and De Nicolo, 2018; Macůrek et al., 2008; Seki et al., 2008b). The finding of PLK1-Apolo1-PP1γ signaling in accurate chromosome segregation demonstrates the complexity and spatiotemporal dynamics of mitotic orchestration in guarding chromosome stability. Future studies will be directed to delineate the structure-activity relationship of Apolo1 and its interaction with PP1γ regulated by phosphorylation.

The response to DNA damage is critical for cellular homeostasis and tissue plasticity control. Using CRISPR-Cas9-based screens, Olivieri et al. (2020) carried out an unbiased and global search for regulators underlying DNA damage response in human cells. They uncovered several important pathways, such as ERCC6L2 and Apolo1 (*C1orf112*), in DNA damage repair. Edogbanya et al. (2021) highlighted the perspective function of Apolo1/*C1orf112* during the revision of this publication, which is consistent with our characterized function of Apolo1 in chromosome stability control. Future studies will also address whether and how PLK1 regulates Apolo1 function in DNA damage repair during the cell division cycle. Proximity ligation coupled withs mass spectrometric identification of Apolo1 networks at different stages of the cell division cycle will likely establish the functional relationships of PLK1-Apolo1-PP1γ in spindle plasticity and chromosome stability control.

In summary, we demonstrate that the evolutionarily conserved, phosphatase-associating protein Apolo1 physically interacts with PLK1 and relays PLK1 signaling in regulation of phosphorylation and accurate chromosome segregation. The PLK1-elicited phosphorylation of Apolo1 negatively regulates PLK1 activity by enabling PP1γ-mediated dephosphorylation. Our findings illustrate a unique molecular mechanism underlying Apolo1-dependent protection of PLK1 inactivation and define a novel role for the PLK1-Apolo1-PP1γ signaling cascade in governing accurate PLK1 kinase activity in space and time to ensure faithful chromosome segregation in mitosis. Altogether, we propose the PLK1-Apolo1-PP1γ feedback loop provides a phosphorylation-elicited dynamic switch for fine-tuning PLK1 activity during early mitosis.

STAR★METHODS

KEY RESOURCES TABLE

REAGENT or RESOURCE	SOURCE	IDENTIFIER
Antibodies		
Rabbit polyclonal anti-C1orf112	Sigma-Aldrich	Cat#HPA024451; RRID:AB_1848667
Rabbit polyclonal anti-C1orf112	This paper	Yanzyme; YZ-0074
Mouse monoclonal anti-PLK1	Invitrogen	Cat#37–7100; RRID:AB_2533336
Rabbit polyclonal anti-pT210-PLK1	Cell Signaling Technology	Cat#9062; RRID:AB_11127447
Rabbit monoclonal anti-PLK1	Cell Signaling Technology	Cat#4513; RRID:AB_2167409
Rabbit monoclonal anti-Cyclin B1	Cell Signaling Technology	Cat#12231; RRID:AB_2783553
Rabbit monoclonal anti-pT288-Aurora A	Cell Signaling Technology	Cat#2914;RRID:AB_2061631
Mouse monoclonal anti-Aurora A	Abcam	Cat#Ab13824; RRID:AB_300667
Rabbit monoclonal anti-Bora	Cell Signaling Technology	Cat#12109; RRID:AB_2797821
Mouse monoclonal anti-pT210-PLK1	Abcam	Cat#Ab39068; RRID:AB_10861033
Goat polyclonal anti-PP1β	Santa Cruz	Cat#Sc-373782; RRID:AB_10916703
Goat polyclonal anti-PP1γ	Santa Cruz	Cat#sc-6208
Mouse monoclonal anti-Mypt1	Santa Cruz	Cat#sc-514261
Mouse monoclonal anti-tubulin	Sigma-Aldrich	Cat#T9026; RRID:AB_477593
Rabbit monoclonal anti-HA	Cell Signaling Technology	Cat#3724; RRID:AB_1549585
Human autoantibody against centromere(ACA)	Immunovision	Cat#HCT-0100; RRID:AB_2744669
Mouse monoclonal anti-MBP	Cell Signaling Technology	Cat#2396; RRID:AB_2140060
Mouse monoclonal anti-GST	Cell Signaling Technology	Cat#2624; RRID:AB_2189875
Mouse monoclonal anti-His	Cell Signaling Technology	Cat#2366; RRID:AB_2115719
Rabbit monoclonal anti-GFP	Cell Signaling Technology	Cat#2037; RRID:AB_1281301
Mouse monoclonal anti-GFP	Sigma-Aldrich	Cat#G6539; RRID:AB_259941
Mouse monoclonal anti-Flag	Sigma-Aldrich	Cat#F1804; RRID:AB_262044
Mouse monoclonal anti-Actin	Abcam	Cat# ab6276; RRID:AB_2223210
Bacterial and virus strains		
Escherichia coli BL21 (DE3) chemically competent cell	AlpaLife	Cat#KTSM104L

REAGENT or RESOURCE	SOURCE	IDENTIFIER
Escherichia coli DH 5α chemically competent cell	AlpaLife	Cat#KTSM101L
Chemicals, peptides, and recombinant proteins		
Lipofectamine 3000	Invitrogen	L300000
RNAi Max	Invitrogen	13778150
MG132	Sigma-Aldrich	SML1135
Thymidine	Sigma-Aldrich	T1895
Nocodazole	Sigma-Aldrich	M1404
Monastrol	Sigma-Aldrich	M8515
BI2536	Selleckchem	S1109
VX-680	Selleckchem	S1048
Recombinant protein GFP-PP1γ with phosphatase activity	This paper	N/A
Recombinant protein PLK1 with kinase activity	This paper	N/A
DAPI	Invitrogen	D1306
Experimental models: Cell lines		
HeLa S3	ATCC	Cat#CCL-2.2
HEK293T	ATCC	Cat#CRL-11268
U2OS	ATCC	Cat#HTB-96
Oligonucleotides		
siApolo1–1#: 5′-CAACAGACAUUCAGCCUUUUU-3′	This paper	N/A
siApolo1–2#: 5′-CAGGAUAUCUCUACUCAAAUU-3′	This paper	N/A
siApolo1-UTR:5′-GGGUUUGAUGCUUUGUCAAdTdT-3′	This paper	N/A
siBora: 5′-CTATGAGACTTCAGATGTAdTdT-3′	This paper	N/A
siPP1γ: 5′-GCAUGAUUUGGAUCAUAUATT-3′	This paper	N/A
siMYPT1: 5′-AGUACUCAACCAUAAUUAATT-3′	This paper	N/A
Recombinant DNA		
GFP-Apolo1-N	This paper	N/A
GFP-Apolo1-M	This paper	N/A
GFP-Apolo1-C	This paper	N/A
GFP-PLK1	Duan et al., 2016	N/A
GFP-PLK1-KD	Duan et al., 2016	N/A
GFP-PLK1-PBD	Duan et al., 2016	N/A
GST-PLK1	This paper	N/A
GST-PLK1-KD	This paper	N/A

REAGENT or RESOURCE	SOURCE	IDENTIFIER
GST-PLK1-PBD	This paper	N/A
GST-Apolo1-N	This paper	N/A
GST-Apolo1-M	This paper	N/A
GST-Apolo1-C	This paper	N/A
GST-PLK1	This paper	N/A
GST-PLK1-PBD	This paper	N/A
MBP-PLK1	This paper	N/A
MBP-Apolo1-WT	This paper	N/A
MBP-Apolo1-WT	This paper	N/A
MBP-Bora	Seki et al., 2008b	N/A
GST-Aurora A	This paper	N/A
GFP-PP1α	This paper	N/A
GFP-PP1β	This paper	N/A
GFP-PP1γ	Liu et al., 2010	N/A
GST-PP1α	This paper	N/A
GST-PP1β	This paper	N/A
GST-PP1γ	This paper	N/A
HA-Flag-Apolo1-WT	This paper	N/A
HA-Flag-Apolo1-S744A	This paper	N/A
HA-Flag-Apolo1-S744D	This paper	N/A
GST-Apolo1-N-S43A	This paper	N/A
GST-Apolo1-N-S43D	This paper	N/A
GFP-Apolo1-N-S43A	This paper	N/A
GFP-Apolo1-N-S43D	This paper	N/A
HA-Flag-Apolo1–4A	This paper	N/A
HA-mCherry-Apolo1-WT	This paper	N/A
HA-mCherry-Apolo1–4A	This paper	N/A
Flag-PLK1	Duan et al., 2016	N/A
Flag-PLK1-PBD	This paper	N/A
Flag-PP1γ	Duan et al., 2016	N/A
pcDNA3.1-HA-Apolo1-WT	This paper	N/A
pcDNA3.1-HA-Apolo1–4A	This paper	N/A
pET28a-Apolo1-C-WT	This paper	N/A
pET28a-Apolo1-C-S744A	This paper	N/A
pET28a-Apolo1-C-S744D	This paper	N/A
pET28a-Apolo1-C-4A	This paper	N/A
pET28a-Cep55	This paper	N/A
Software and algorithms		
ImageJ	National Institutes of Health	https://imagej.nih.gov/ij/

REAGENT or RESOURCE	SOURCE	IDENTIFIER
Blastn	National Center for Biotechnology Information	https://blast.ncbi.nlm.nih.gov/Blast.cgi?PAGE_TYPE=BlastSearch
GraphPad Prism	GraphPad Software, Inc.	https://www.graphpad.com/scientific-software/prism/
Adobe Illustrator	Adobe Systems, Inc.	https://www.adobe.com/
Thermo proteome Discoverer (1.4.1.14)	Thermo Fisher	N/A
MaxQuant software (1.6.0.1)	MaxQuant	https://www.maxquant.org/

RESOURCE AVAILABILITY

Lead contact—Further information and requests for resources and reagents should be directed to and will be fulfilled by the lead contact, Xuebiao Yao (yaoxb@ustc.edu.cn)

Materials availability—All unique/stable reagents generated in this study are available from the lead contact without restriction.

Data and code availability—This study did not generate any unique datasets or code.

EXPERIMENTAL MODEL AND SUBJECT DETAILS

Cell lines—HeLa S3 and HEK293T cells (from ATCC), were cultured and maintained in advanced Dulbecco's Modified Eagle's Medium (DMEM, Invitrogen) with 10% (vol/vol) fetal bovine serum (FBS, HyClone), 2 mM glutamine and 100 units/mL penicillin plus 100 μg/mL streptomycin (Invitrogen) at 37°C with 5% CO_2. U2OS cell line (from ATCC) was cultured and maintained in McCoy5A with 10% (vol/vol) fetal bovine serum (FBS, HyClone), 2 mM glutamine and 100 units/mL penicillin plus 100 μg/mL streptomycin (Invitrogen) at 37°C with 5% CO_2. LAP-Apolo1 and LAP-PLK1 stable cell lines were kindly gifted by Anthony Hyman Lab from Max Plank Institute in Germany. All the cell lines were tested for mycoplasma contamination using the MycoAlert mycoplasma detection kit (Lonza, Switzerland).

Bacterial strains—*Escherichia* coli BL21 (DE3) and DH 5a chemically competent cells were obtained from AlpaLife (Cat#KTSM104L and KTSM101L).

METHOD DETAILS

Plasmids—To generate all the plasmids used in this study, PCR-amplified cDNA was cloned into corresponding vectors. Specifically, the bacterial-expressed constructs of Apolo1 and Bora were cloned into pMal-C2 vector (New England Biolabs, Beverly, MA). Bacterial expression constructs of GST-PP1 α,β,γ and Aurora A were cloned into pGEX-6P-1 (GE Healthcare). Bacterial-expressed constructs of GST-PLK1 and GST-Apolo1 full length and truncations were also cloned into pGEX-6P-1 (GE Healthcare). To generate Flag-tag protein, PLK1, PP1γ and Apolo1 cDNA were inserted into the p3 × Flag-myc-CMV-24 vector (Sigma-Aldrich). mCherry-H2B fusion protein was cloned into pcDNA3.1 vector. GFP-tagged PLK1, Apolo1 full-length and truncations were inserted into pEGFP-C1 vector (Clontech). mCherry-Apolo1 and HA-Apolo1 were cloned into pcDNA3.1 vector. Hec1-

PLK1 sensor plasmid was described previously (Liu et al., 2012). All site(s) specific mutations were generated using the Vazyme mutagenesis Kit (C214–01, Vazyme Inc.) according to manual instructions. All plasmid constructs were sequenced for verification.

Cell transfection, drug treatments and antibody preparation—HeLa cells were transfected with plasmids, siRNA (20 nM) or shRNA using Lipofectamine 3000 (Invitrogen) or RNAi Max (Invitrogen). For mitotic synchronization, cells were blocked at G1/S phase in 2 mM thymidine (Sigma-Aldrich) for 16 hr, followed by release in fresh medium for indicated hr. In some specific experiments, cells were treated with indicated inhibitors for another 1 or 2 hr, wherein BI2536 was used at 100 nM; MG132 was used at 20 μM. Rabbit peptide antibodies against the 736–750 amino acids of Apolo1 were generated by YanZym LLC and affinity purified against peptide-conjugated Sepharose beads as described previously (Yao et al., 1997).

Immunofluorescence microscopy and data analyses—Cells grown on coverslips were fixed with 3.7% formaldehyde (Sigma-Aldrich) in PHEM (60 mM PIPES, 25 mM HEPES, pH 6.9, 10 mM EGTA, 2 mM $MgCl_2$, and 4 M Glycerol)/PBS at 37°C for 10 min. After formaldehyde fixation, cells were subsequently permeabilized with 0.1% Triton X-100 in PBS at room temperature for 10 min. Following 30-min block in 1% BSA and incubation with primary antibodies at room temperature for 1 hr, cells were incubated with secondary antibodies for another 1 hr. After staining with 4, 6-diamidino-2-phenylindole (DAPI, Sigma-Aldrich) for 1–2 min, coverslips were mounted in vectashield mounting medium (Vector). Images were acquired using Olympus 60 × NA1.42 Plan APON objective on an Olympus IX71 microscope (Applied Precision Inc.). Decon-voluted images from each focal plane were projected into a single stack montage using SoftWorx software (Applied Precision).

Fluorescence intensity quantification—For fluorescence intensity quantification of the level of kinetochore-associated protein, the kinetochore staining signals were measured with ImageJ software (NIH), according to the procedures described previously (Mo et al., 2016). In brief, the average pixel intensities from at least 50 kinetochore pairs from five cells were measured, and the background pixel intensities were subtracted. The pixel intensities at each kinetochore pair were then normalized against ACA pixel values to account for any variations in staining or image acquisition.

FRET sensor assay—Live fluorescence ratio imaging was collected using a live cell microscopy imaging system built on a Nikon Ti-Eclipse inverted microscope equipped with a 100 × / NA1.40 Plan Apo oil immersion lens (Nikon), a charge-coupled device camera (Andor), a spinning disk confocal (Yokogawa), an XY-piezo Z stage (Prior NanoScan Z), and a laser merge module (ILE, Andor) controlled by iQ3 software (Andor). For live-cell imaging of FRET sensors, TFP was excited at 445 nm, while TFP and YFP (FRET channel) emissions were simultaneously acquired with a beam splitter (Optosplit II, Cairn Research Ltd). Images of cells were collected as confocal image stacks (five planes, 0.5-μm spacing). For data analysis images with YFP and CFP signal were cropped in ImageJ first, and then the FRET emission ratio (TFP/YFP) was calculated by using custom software written

in MATLAB as previous described (Liu et al., 2009). Individual kinetochore was defined automatically from images presented as maximal intensity projections of confocal stacks, and FRET emission ratio was calculated on each kinetochore. According to the design of the FRET-based sensors, a higher FRET emission ratio indicates a lower kinase activity.

Live cell microscopy and data analyses—Live cell imaging was performed as described previously (Mo et al., 2016). In brief, cells were cultured in MatTek glass-bottom dishes (MatTek) in CO_2-independent medium (GIBCO) containing 10% (vol/vol) FBS and 2 mM glutamine in a sealed chamber heated to 37°C and observed under a DeltaVision deconvolution microscope (Applied Precision). Images were acquired from NEBD with 5 min intervals and presented in Photoshop and Illustrator (Adobe).

Immunoprecipitation and pull-down assay—For co-immunoprecipitation assay, HEK293T or HeLa cells were transfected with indicated plasmids, collected, and lysed in a lysis buffer (50 mM Tris-HCl, pH 7.4; 150 mM NaCl; 1 mM EDTA) containing 0.1% Triton X-100 in the presence of mammalian protease inhibitors cocktail (P8340, Sigma-Aldrich). After clarification by centrifugation, cell lysates were incubated with Flag M2 beads (F2426, Sigma-Aldrich) at 4°C rotating for 3 hr. In immunoprecipitation of endogenous PLK1, HeLa cell lysates were incubated with IgG or PLK1 antibody at 4°C rotating for 4 hr followed by extended incubation with protein A/G microbeads for another 1 hr. After incubation, the beads were washed three times with lysis buffer containing 0.1% Triton X-100 and washed one time with lysis buffer and then boiled in 1 × SDS-PAGE (SDS-polyacrylamide gel) sample buffer. For co-immunoprecipitation assay of GFP-Apolo1-N WT and Ser43 mutants along with Flag-PLK1-PBD, mitotic HeLa cells were lysed in a lysis buffer (50 mM Tris-HCl, pH 7.4; 150 mM NaCl; 1 mM EDTA) containing 0.5% Triton X-100. The lysates were incubated with Flag M2 beads and the beads were washed three times with lysis buffer containing 0.5% Triton X-100 after incubation. The bound proteins were separated on an SDS-PAGE gel and transferred onto nitrocellulose membrane for western blotting analyses.

Pull-down assays were carried out as described previously (Xia et al., 2012). Briefly, the GST-tagged proteins in the soluble fraction were purified from bacteria by glutathione-agarose chromatography or followed by eluting with GST elution buffer (50 mM Tris-HCl, 10 mM reduced glutathione, pH 8.0), whereas MBP-tagged proteins were purified using Amylose beads (New England Biolabs). MBP-tagged protein-bound Sepharose beads were incubated with purified GST-tagged proteins for 1 hr at 4°C. After incubation, the beads were washed three times with PBS containing 0.1% Triton X-100 and one time with PBS and then boiled in 1 × SDS-PAGE sample buffer. The bound proteins were separated by SDS-PAGE followed by CBB (Coomassie brilliant blue) staining or western blotting analyses using GST antibody.

Production of active PLK1 kinase—To assay the activation of His-PLK1 by GST-Aurora A and MBP-Bora, His-Plk1 was incubated with or without GST-Aurora A and MBP-Bora/MBP in the presence of unlabeled ATP in 50 μL kinase reaction buffer for 30 min at room temperature as described (Seki et al., 2008b). A portion of the samples was analyzed for phosphorylation of PLK1-T210 by western blotting with pT210-PLK1 antibody. The remaining His-PLK1 was centrifuged by using the anti-GST or maltose agarose beads to

remove the GST-Aurora A and MBP-Bora. The supernatant of the reaction system was active His-PLK1 kinase, which was then assayed for the PLK1 kinase activity.

Production of active PP1γ phosphatase—PP1γ phosphatase was isolated from a strain of E.coli that carries the coding sequence for human PP1γ under the control of the trp-lac hybrid promoter within pGEX-6P-1 vector (Dohadwala and Berndt, 1998; Zhang et al., 1992). Briefly, after purification with GST beads, GST-PP1γ proteins was eluted with NEB buffer containing 10 mM GSH and GST tag was subsequently removed by PreScission Protease as described (Liu et al., 2010). PreScission Protease and cleaved GST tags were removed by GST beads after centrifugation and the supernatants were active PP1γ phosphatase.

In vitro* phosphorylation—In vitro* phosphorylation assays were carried out as described previously (Duan et al., 2016). The PLK1 kinase (7728) was purchased from Cell Signaling Technology. The kinase reactions were performed in 40 μL of1 × kinase buffer (25 mM HEPES, pH 7.2, 50 mM NaCl, 2 mM EGTA, 5 mM $MgSO_4$, 1 mM DTT, 0.01% Brij35) containing 200 ng PLK1 kinase, 3–5 μg MBP-tagged proteins, 5 μCi [γ–^{32}P]-ATP and 50 μM ATP. The mixtures were incubated at 30°C for 30 min, and the reactions were stopped with 5 × SDS-PAGE sample buffer. Proteins were separated by SDS-PAGE and detected by subsequent autoradiography.

Kinase assay—The kinetics of PLK1 was characterized by the Amplite™ Universal Fluorimetric Kinase Assay Kit (AAT Bioquest) according to the manufacturer's manual as previously reported (Huang et al., 2019). 50 nM PLK1 was incubated with indicated concentrations of casein in 20 μL kinetics assay buffer (60 mM HEPES, pH 7.5; 3 mM $MgCl_2$; 3 mM $MnCl_2$; 3 μM Na-orthovanadate) at 37 °C for 30 min. ADP sensor and sensor buffer were added into the preparations, which were incubated for another 15 min at room temperature. The amount of ADP produced from the kinase reaction was detected by monitoring fluorescence intensity at Ex/Em = 540/590 nm on TECAN Genios Plus. K_m and k_{cat} values were calculated according to the Michaelis-Menten equation. In the case of activation of PLK1 by Aurora A and Bora, the priming reaction was initiated 5 min prior to the addition of Apolo1.

***In vitro* dephosphorylation assays—**PP1γ phosphatase was generated as previously described (Dohadwala and Berndt, 1998). Autophosphorylated GST-Aurora A was purified as described (Seki et al., 2008b). 5 pmol of His-PLK1 kinase was incubated with 0.5 pmol PP1γ without or with the indicated concentration of MBP-Apolo1 in 1 × NEBuffer for PMP (Protein MetalloPhosphatases, P0754S, New England Biolabs), supplemented with 1 mM $MnCl_2$ and 1 mM protease inhibitors at 30°C for 30 min to 2 hr, according to the procedures described previously (Duan et al., 2016). The reactions were stopped with 5 × SDS-PAGE sample buffer. Proteins were separated by SDS-PAGE, analyzed by western blotting with pT210-PLK1 and PLK1 antibodies and visualized with ECL reagent (Thermo Scientific Pierce) on a LAS400 imaging system (GE Healthcare). Signal intensities were quantified using ImageJ software (NIH), according to the procedures described previously (Mo et al., 2016). His-PLK1 kinase dephosphorylation was determined by measuring the

dephosphorylation in the presence of PP1γ/Apolo1 and subtracted from the experiments in the absence of PP1γ.

MS sample preparation and analysis—The Flag immunoprecipitation and wash conditions were described in 'Immunoprecipitation and pull-down assay'. After washing, the samples were reduced with 10 mM DTT in 50 mM Ammonium bicarbonate (ABC) at 56°C for 30 min and then alkylated with 30 mM of iodoacetamide (IAA) for 30 min. After above, 2 μg of trypsin (Promega, V511A) was added to samples for overnight digestion at 37°C. After trypsin digestion, the peptide samples were desalted and analyzed with Thermo Fisher Q Exactive mass spectrometer equipped with Easy-nanoLC, followed by a scan range of m/z 350–1550. The raw files were analyzed with MaxQuant software (1.6.0.1) and Thermo proteome Discoverer (1.4.1.14). The human database was from Uniprot (Proteome ID: UP000005640). Phosphorylation (S/T, +79.9663Da) and Oxidation (M, +15.9949Da) modification were included as variable modification. Carbamidomethyl (C, +57.0215Da) was set as fix modification.

Bioinformatics studies—Two bioinformatics tools were used to predict potential related mitotic factors. First, co-expression prediction tool developed by van Dam et al. (2012) was used to find out potential genes involved in the mitotic kinases-phosphatases network. PLK1 kinase and phosphatases PP1α, PP1β, PP1γ were used as the seeds for co-expression prediction respectively. 1547 genes which were ''friends'' with all four seeds were selected for further functional analysis. The Gene Ontology (GO) term finder web-server developed at the Lewis-Sigler Institute at Princeton were used to cluster all overlap genes depending on common functions (Boyle et al., 2004). *P value* cutoff was set as $p > 0$ (default) for the clustering. 17 genes which were found to be uncharacterized were examined and checked manually. Pseudogene and RNA coding genes were filtered out, Apolo1 (*C1orf112*) was selected for further experimental and function analyses based on its co-expression profile with PLK1 and its PP1-binding motif.

QUANTIFICATION AND STATISTICAL ANALYSIS

All statistics were described in the figure legends. Two-sided unpaired Student's t test was applied for experimental comparisons (using GraphPad Prism 7), differences were considered significant when p was < 0.05. All western blotting analyses were taken from three separated experiments unless otherwise stated. No statistical method was used to predetermine sample size. All data were expected to have normal distribution.

Supplementary Material

Refer to Web version on PubMed Central for supplementary material.

ACKNOWLEDGMENTS

We thank the members of our groups for insightful discussions during the course of this study. This work was supported by the National Key Research and Development Program of China (2017YFA0503600, 2016YFA0100500, and 2016YFA0101200), Chinese Natural Science Foundation grants (31621002, 32090040, 21922706, 91854203, 91853115, 81630080, 31871359, 21778050, 91749125, 31430054, 31970655, and 31471275), the Ministry of Education (IRT_17R102 and 20113402130010), the Strategic Priority Research Program of the Chinese Academy of Sciences (XDB19000000), the Fundamental Research Funds for the Central

Universities (WK2070000194), a Anhui Province Key Project grant (08040102005), the Chinese Academy of Sciences Center of Excellence (2015HSC-UE010), a Anhui Provincial Natural Science Foundation grant (1508085SMC213), and the independent Innovation Foundation of the University of Science and Technology of China (WK2070000111, YD2070006001, and WK2070000123). This work was also supported in part by National Institutes of Health (United States) grants (CA164133, DK115812, and DK56292) and the European Commission's Seventh Framework Program (FP7-HEALTH-2009–241548, MitoSys). M.A. is a CSC fellow.

REFERENCES

Ahonen LJ, Kallio MJ, Daum JR, Bolton M, Manke IA, Yaffe MB, Stukenberg PT, and Gorbsky GJ (2005). Polo-like kinase 1 creates the tension-sensing 3F3/2 phosphoepitope and modulates the association of spindle-checkpoint proteins at kinetochores. Curr. Biol 15, 1078–1089. [PubMed: 15964272]

Archambault V, and Glover DM (2009). Polo-like kinases: conservation and divergence in their functions and regulation. Nat. Rev. Mol. Cell Biol 10, 265–275. [PubMed: 19305416]

Boyle EI, Weng S, Gollub J, Jin H, Botstein D, Cherry JM, and Sherlock G. (2004). GO:TermFinder—open source software for accessing Gene Ontology information and finding significantly enriched Gene Ontology terms associated with a list of genes. Bioinformatics20, 3710–3715. [PubMed: 15297299]

Bruinsma W, Macůrek L, Freire R, Lindqvist A, and Medema RH (2014). Bora and Aurora-A continue to activate Plk1 in mitosis. J. Cell Sci 127, 801–811. [PubMed: 24338364]

Chiyoda T, Sugiyama N, Shimizu T, Naoe H, Kobayashi Y, Ishizawa J, Arima Y, Tsuda H, Ito M, Kaibuchi K, et al. (2012). LATS1/WARTS phosphorylates MYPT1 to counteract PLK1 and regulate mammalian mitotic progression. J. Cell Biol 197, 625–641. [PubMed: 22641346]

Chu L, Zhu T, Liu X, Yu R, Bacanamwo M, Dou Z, Chu Y, Zou H, Gibbons GH, Wang D, et al. (2012). SUV39H1 orchestrates temporal dynamics of centromeric methylation essential for faithful chromosome segregation in mitosis. J. Mol. Cell Biol 4, 331–340. [PubMed: 22831836]

Cleveland DW, Mao Y, and Sullivan KF (2003). Centromeres and kinetochores: from epigenetics to mitotic checkpoint signaling. Cell 112, 407–421. [PubMed: 12600307]

de Lichtenberg U, Jensen LJ, Brunak S, and Bork P. (2005). Dynamic complex formation during the yeast cell cycle. Science307, 724–727. [PubMed: 15692050]

Dohadwala M, and Berndt N. (1998). Expression of functional protein phosphatase 1 catalytic subunit in E. coli. In Protein Phosphatase Protocols, Ludlow JW, ed. (Springer), pp. 191–199.

Duan H, Wang C, Wang M, Gao X, Yan M, Akram S, Peng W, Zou H, Wang D, Zhou J, et al. (2016). Phosphorylation of PP1 regulator Sds22 by PLK1 ensures accurate chromosome segregation. J. Biol. Chem 291, 21123–21136. [PubMed: 27557660]

Dumitru AMG, Rusin SF, Clark AEM, Kettenbach AN, and Compton DA (2017). Cyclin A/Cdk1 modulates Plk1 activity in prometaphase to regulate kinetochore-microtubule attachment stability. eLife 6, e29303. [PubMed: 29154753]

Edogbanya J, Tejada-Martinez D, Jones NJ, Jaiswal A, Bell S, Cordeiro R, van Dam S, Rigden DJ, and de Magalhães JP (2021). Evolution, structure and emerging roles of C1ORF112 in DNA replication, DNA damage responses, and cancer. Cell. Mol. Life Sci 78, 4365–4376. [PubMed: 33625522]

Elia AE, Cantley LC, and Yaffe MB (2003). Proteomic screen finds pSer/pThr-binding domain localizing Plk1 to mitotic substrates. Science 299, 1228–1231. [PubMed: 12595692]

Fang L, Seki A, and Fang G. (2009). SKAP associates with kinetochores and promotes the metaphase-to-anaphase transition. Cell Cycle8, 2819–2827. [PubMed: 19667759]

Foley EA, and Kapoor TM (2013). Microtubule attachment and spindle assembly checkpoint signalling at the kinetochore. Nat. Rev. Mol. Cell Biol 14, 25–37. [PubMed: 23258294]

Godek KM, Kabeche L, and Compton DA (2015). Regulation of kinetochore-microtubule attachments through homeostatic control during mitosis. Nat. Rev. Mol. Cell Biol 16, 57–64. [PubMed: 25466864]

Hendrickx A, Beullens M, Ceulemans H, Den Abt T, Van Eynde A, Nicolaescu E, Lesage B, and Bollen M. (2009). Docking motif-guided mapping of the interactome of protein phosphatase-1. Chem. Biol16, 365–371. [PubMed: 19389623]

Huang Y, Lin L, Liu X, Ye S, Yao PY, Wang W, Yang F, Gao X, Li J, Zhang Y, et al. (2019). BubR1 phosphorylates CENP-E as a switch enabling the transition from lateral association to end-on capture of spindle microtubules. Cell Res 29, 562–578. [PubMed: 31201382]

Joukov V, and De Nicolo A. (2018). Aurora-PLK1 cascades as key signaling modules in the regulation of mitosis. Sci. Signal11, eaar4195. [PubMed: 30108183]

Joukov V, Walter JC, and De Nicolo A. (2014). The Cep192-organized aurora A-Plk1 cascade is essential for centrosome cycle and bipolar spindle assembly. Mol. Cell55, 578–591. [PubMed: 25042804]

Lampson MA, and Cheeseman IM (2011). Sensing centromere tension: Aurora B and the regulation of kinetochore function. Trends Cell Biol 21, 133–140. [PubMed: 21106376]

Lampson MA, and Kapoor TM (2005). The human mitotic checkpoint protein BubR1 regulates chromosome-spindle attachments. Nat. Cell Biol 7, 93–98. [PubMed: 15592459]

Lénárt P, Petronczki M, Steegmaier M, Di Fiore B, Lipp JJ, Hoffmann M, Rettig WJ, Kraut N, and Peters JM (2007). The small-molecule inhibitor BI 2536 reveals novel insights into mitotic roles of polo-like kinase 1. Curr. Biol 17, 304–315. [PubMed: 17291761]

Liu D, Vader G, Vromans MJ, Lampson MA, and Lens SM (2009). Sensing chromosome bi-orientation by spatial separation of aurora B kinase from kinetochore substrates. Science 323, 1350–1353. [PubMed: 19150808]

Liu D, Vleugel M, Backer CB, Hori T, Fukagawa T, Cheeseman IM, and Lampson MA (2010). Regulated targeting of protein phosphatase 1 to the outer kinetochore by KNL1 opposes Aurora B kinase. J. Cell Biol 188, 809–820. [PubMed: 20231380]

Liu D, Davydenko O, and Lampson MA (2012). Polo-like kinase-1 regulates kinetochore-microtubule dynamics and spindle checkpoint silencing. J. Cell Biol 198, 491–499. [PubMed: 22908307]

Liu X, Liu X, Wang H, Dou Z, Ruan K, Hill DL, Li L, Shi Y, and Yao X. (2020). Phase separation drives decision making in cell division. J. Biol. Chem295, 13419–13431. [PubMed: 32699013]

Macůrek L, Lindqvist A, Lim D, Lampson MA, Klompmaker R, Freire R, Clouin C, Taylor SS, Yaffe MB, and Medema RH (2008). Polo-like kinase-1 is activated by aurora A to promote checkpoint recovery. Nature 455, 119–123. [PubMed: 18615013]

Meiselbach H, Sticht H, and Enz R. (2006). Structural analysis of the protein phosphatase 1 docking motif: molecular description of binding specificities identifies interacting proteins. Chem. Biol13, 49–59. [PubMed: 16426971]

Mertins P, Yang F, Liu T, Mani DR, Petyuk VA, Gillette MA, Clauser KR, Qiao JW, Gritsenko MA, Moore RJ, et al. (2014). Ischemia in tumors induces early and sustained phosphorylation changes in stress kinase pathways but does not affect global protein levels. Mol. Cell. Proteomics 13, 1690–1704. [PubMed: 24719451]

Mertins P, Mani DR, Ruggles KV, Gillette MA, Clauser KR, Wang P, Wang X, Qiao JW, Cao S, Petralia F, et al.; NCI CPTAC (2016). Proteogenomics connects somatic mutations to signalling in breast cancer. Nature 534, 55–62. [PubMed: 27251275]

Mo F, Zhuang X, Liu X, Yao PY, Qin B, Su Z, Zang J, Wang Z, Zhang J, Dou Z, et al. (2016). Acetylation of Aurora B by TIP60 ensures accurate chromosomal segregation. Nat. Chem. Biol 12, 226–232. [PubMed: 26829474]

Nasa I, Rusin SF, Kettenbach AN, and Moorhead GB (2018). Aurora B opposes PP1 function in mitosis by phosphorylating the conserved PP1-binding RVxF motif in PP1 regulatory proteins. Sci. Signal 11, eaai8669. [PubMed: 29764992]

Olivieri M, Cho T, Álvarez-Quilón A, Li K, Schellenberg MJ, Zimmermann M, Hustedt N, Rossi SE, Adam S, Melo H, et al. (2020). A Genetic Map of the Response to DNA Damage in Human Cells. Cell 182, 481–496.e21. [PubMed: 32649862]

Rhodes DR, Yu J, Shanker K, Deshpande N, Varambally R, Ghosh D, Barrette T, Pandey A, and Chinnaiyan AM (2004). Large-scale meta-analysis of cancer microarray data identifies common transcriptional profiles of neoplastic transformation and progression. Proc. Natl. Acad. Sci. USA 101, 9309–9314. [PubMed: 15184677]

Segal E, Friedman N, Koller D, and Regev A. (2004). A module map showing conditional activity of expression modules in cancer. Nat. Genet36, 1090–1098. [PubMed: 15448693]

Seki A, Coppinger JA, Du H, Jang C-Y, Yates JR 3rd, and Fang G. (2008a). Plk1- and b-TrCP-dependent degradation of Bora controls mitotic progression. J. Cell Biol181, 65–78. [PubMed: 18378770]

Seki A, Coppinger JA, Jang C-Y, Yates JR, and Fang G. (2008b). Bora and the kinase Aurora a cooperatively activate the kinase Plk1 and control mitotic entry. Science320, 1655–1658. [PubMed: 18566290]

Stuart JM, Segal E, Koller D, and Kim SK (2003). A gene-coexpression network for global discovery of conserved genetic modules. Science 302, 249–255. [PubMed: 12934013]

van Dam S, Cordeiro R, Craig T, van Dam J, Wood SH, and de Magalhães JP (2012). GeneFriends: an online co-expression analysis tool to identify novel gene targets for aging and complex diseases. BMC Genomics 13, 535. [PubMed: 23039964]

Whitfield ML, Sherlock G, Saldanha AJ, Murray JI, Ball CA, Alexander KE, Matese JC, Perou CM, Hurt MM, Brown PO, and Botstein D. (2002). Identification of genes periodically expressed in the human cell cycle and their expression in tumors. Mol. Biol. Cell13, 1977–2000. [PubMed: 12058064]

Wong J, and Fang G. (2006). HURP controls spindle dynamics to promote proper interkinetochore tension and efficient kinetochore capture. J. Cell Biol173, 879–891. [PubMed: 16769820]

Xia P, Wang Z, Liu X, Wu B, Wang J, Ward T, Zhang L, Ding X, Gibbons G, Shi Y, and Yao X. (2012). EB1 acetylation by P300/CBP-associated factor (PCAF) ensures accurate kinetochore-microtubule interactions in mitosis. Proc. Natl. Acad. Sci. USA109, 16564–16569. [PubMed: 23001180]

Yamashiro S, Yamakita Y, Totsukawa G, Goto H, Kaibuchi K, Ito M, Hartshorne DJ, and Matsumura F. (2008). Myosin phosphatase-targeting subunit 1 regulates mitosis by antagonizing polo-like kinase 1. Dev. Cell14, 787–797. [PubMed: 18477460]

Yao X, Anderson KL, and Cleveland DW (1997). The microtubule-dependent motor centromere-associated protein E (CENP-E) is an integral component of kinetochore corona fibers that link centromeres to spindle microtubules. J. Cell Biol 139, 435–447. [PubMed: 9334346]

Yu R, Wu H, Ismail H, Du S, Cao J, Wang J, Ward T, Yang F, Gui P, Ali M, et al. (2020). Methylation of PLK1 by SET7/9 ensures accurate kinetochore-microtubule dynamics. J. Mol. Cell Biol 12, 462–476. [PubMed: 31863092]

Zhang AJ, Bai G, Deans-Zirattu S, Browner MF, and Lee EY (1992). Expression of the catalytic subunit of phosphorylase phosphatase (protein phosphatase-1) in Escherichia coli. J. Biol. Chem 267, 1484–1490. [PubMed: 1730696]

Zhang L, Shao H, Huang Y, Yan F, Chu Y, Hou H, Zhu M, Fu C, Aikhionbare F, Fang G, et al. (2011). PLK1 phosphorylates mitotic centromere-associated kinesin and promotes its depolymerase activity. J. Biol. Chem 286, 3033–3046. [PubMed: 21078677]

Zhou H, Di Palma S, Preisinger C, Peng M, Polat AN, Heck AJ, and Mohammed S. (2013). Toward a comprehensive characterization of a human cancer cell phosphoproteome. J. Proteome Res12, 260–271. [PubMed: 23186163]

Zitouni S, Nabais C, Jana SC, Guerrero A, and Bettencourt-Dias M. (2014). Polo-like kinases: structural variations lead to multiple functions. Nat. Rev. Mol. Cell Biol15, 433–452. [PubMed: 24954208]

Highlights

- Apolo1 is a substrate of PLK1 and colocalizes to kinetochore during prometaphase
- Apolo1 interacts with PP1γ, and the interaction is disrupted by PLK1 phosphorylation
- Disruption of PP1γ-Apolo1 interaction inactivates PLK1 by T-loop dephosphorylation
- Apolo1 provides feedback control of PLK1 activity in mitosis

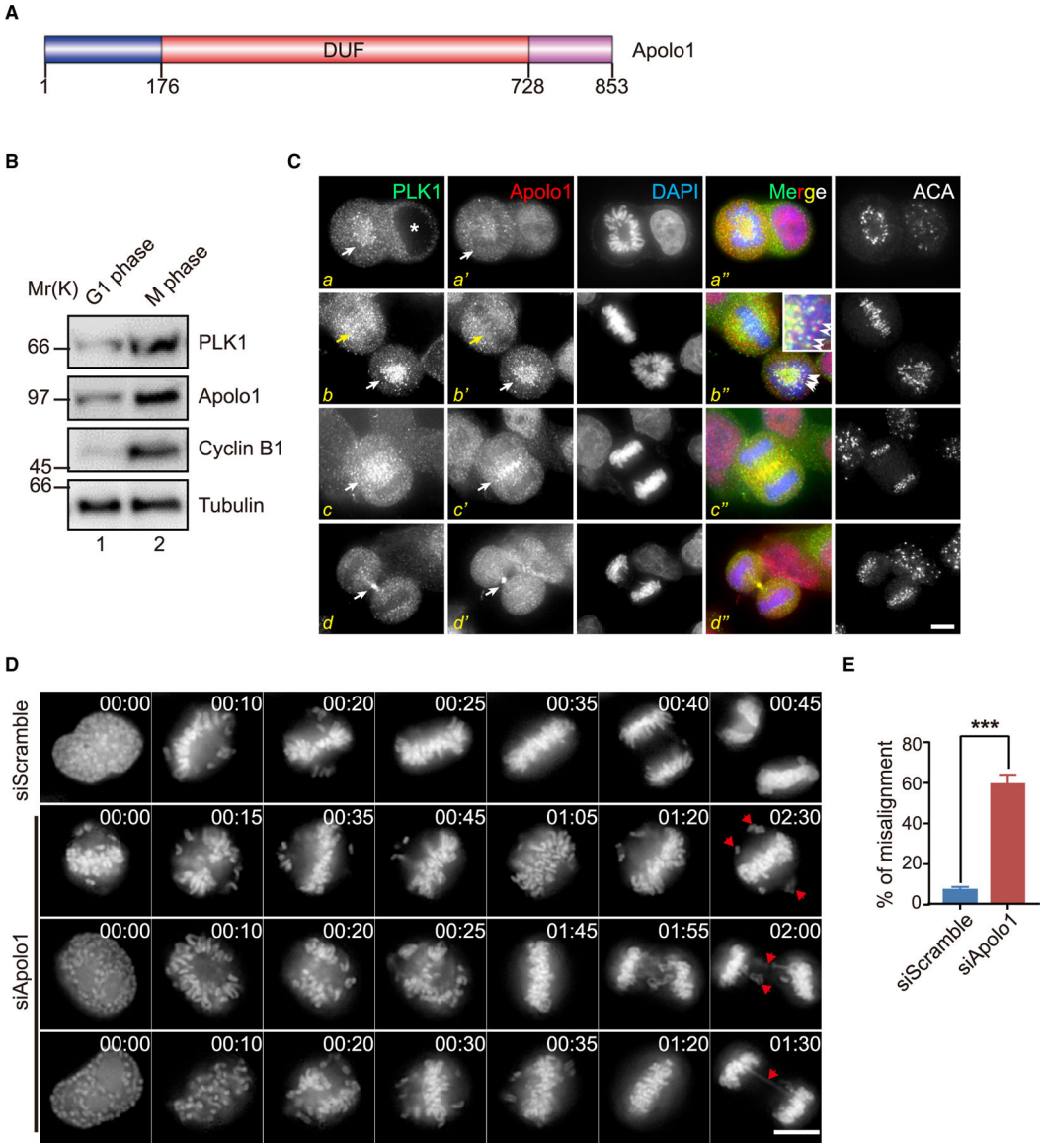

Figure 1. Apolo1 is a new PLK1-interacting protein essential for faithful mitosis

(A) Schematic illustration of the Apolo1 structure and domains. Apolo1 contains no characterized structural motifs. DUF annotates a domain of unknown function.

(B) Western blotting analyses of Apolo1 and related proteins in interphase and mitotic HeLa cells.

(C) Representative immunofluorescence images showing Apolo1 and PLK1 localization in different mitotic stages. Centromeres are identified using anti-centromere antibodies (ACAs). The asterisk indicates the nucleus; arrowheads indicate the colocalization. Scale bar, 10 μm. The distribution of Apolo1 is superimposed onto that of PLK1 in the prometaphase kinetochore (b").

(D) Representative mitotic phenotypes in HeLa cells expressing siApolo1 or siScramble (control siRNA) shown by time-lapse imaging and visualized with mCherry-H2B (mCh-H2B) (red arrowheads indicate chromosome misalignments, lagging chromosomes, and

chromosomes bridges; numbers at the upper right of images indicate elapsed time in hours and minutes). Scale bar, 10 μm.

(E) Quantification of chromosome segregation defects of live HeLa cells transfected with siScramble (n = 89) or siApolo1 (n = 99) as in (D). Cells exhibiting unaligned chromosomes and failing to align at the metaphase plate within 60 min after nuclear envelope breakdown (NEBD) were considered misaligned (D, second panel). Data represent mean ± SEM from three independent experiments. Statistical significance was tested by two-sided t test; ***$p < 0.001$.

See also Figure S1.

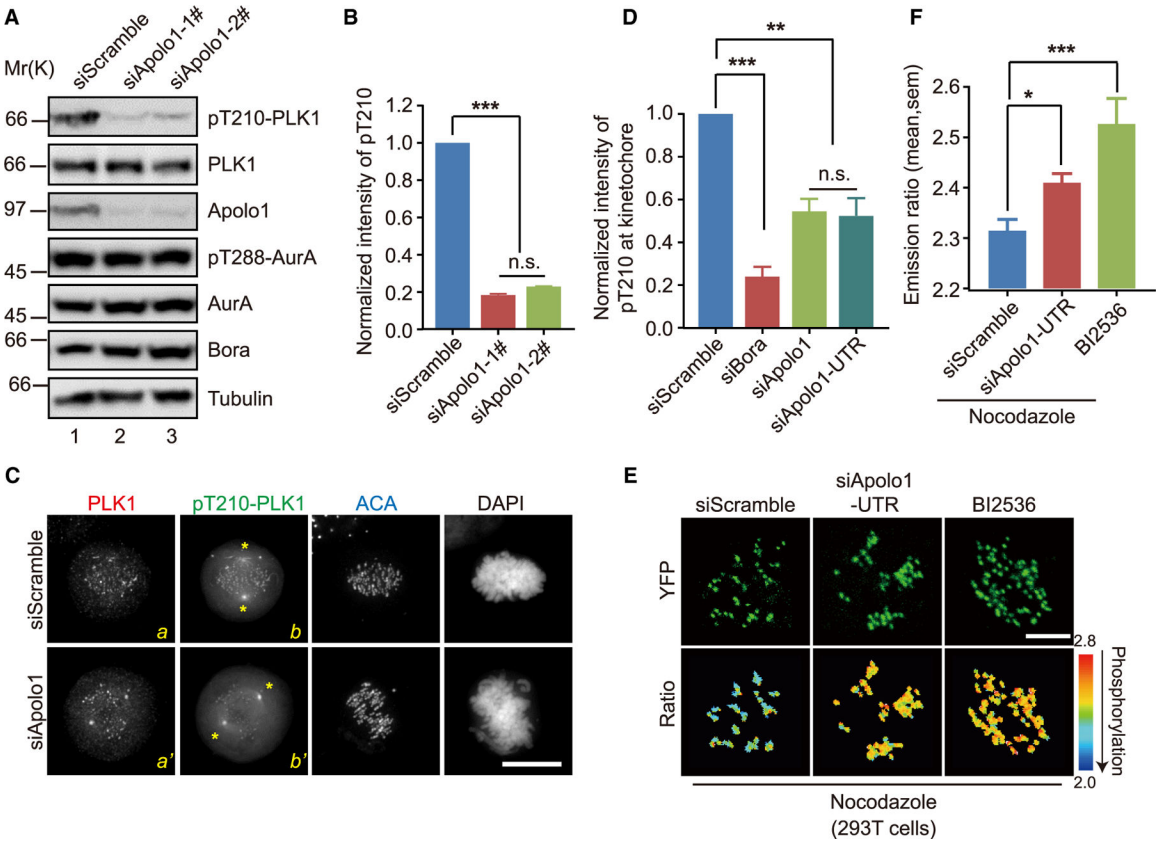

Figure 2. Apolo1 is important for sustaining PLK1 activity in mitotic cells

(A) Mitotic HeLa cells treated with two independent Apolo1 siRNAs were collected by shake-off, separated by SDS-PAGE, and blotted with the indicated antibodies against Apolo1, pT210-PLK1, PLK1, pT288-Aurora A, Aurora A, Bora, and tubulin.

(B) Quantification of pT210-PLK1 intensity (relative to PLK1) in (A).

(C) Immunofluorescence staining of pT210-PLK1, PLK1, and ACA in prometaphase HeLa cells transfected with siScramble and siApolo1. Suppression of Apolo1 did not alter the kinetochore distribution of PLK1 but attenuated the pT210-PLK1 labeling (asterisks indicate pT210-PLK1 located at centrosomes). Scale bar, 10 μm.

(D) Quantification of the relative pT210-PLK1 level (pT210-PLK1/PLK1) at the kinetochore in (C). Data represent mean ± SEM and were examined with two-sided t test. A total of 150 pairs of kinetochores from at least 10 cells were examined from three independent experiments. Statistical significance was tested by two-sided t test; $^{**}p < 0.01$, $^{***}p < 0.001$.

(E) Control or Apolo1-depleted 293T cells expressing the Hec1-targeted PLK1 kinase sensor were imaged at prometaphase. 293T cells were synchronized with 100 ng/mL nocodazole for 2 h after release from single thymidine treatment. BI2536 was added at 100 nM for 0.5 h. Scale bar, 5 μm.

(F) Statistical analyses of the FRET/CFP emission ratio as in (E). At least 20 cells of each group were calculated, and data represent mean ± SEM from three independent experiments. Statistical significance was tested by two-sided t test and represented by asterisks corresponding to $^{*}p < 0.05$ and $^{***}p < 0.001$.

See also Figures S1 and S2.

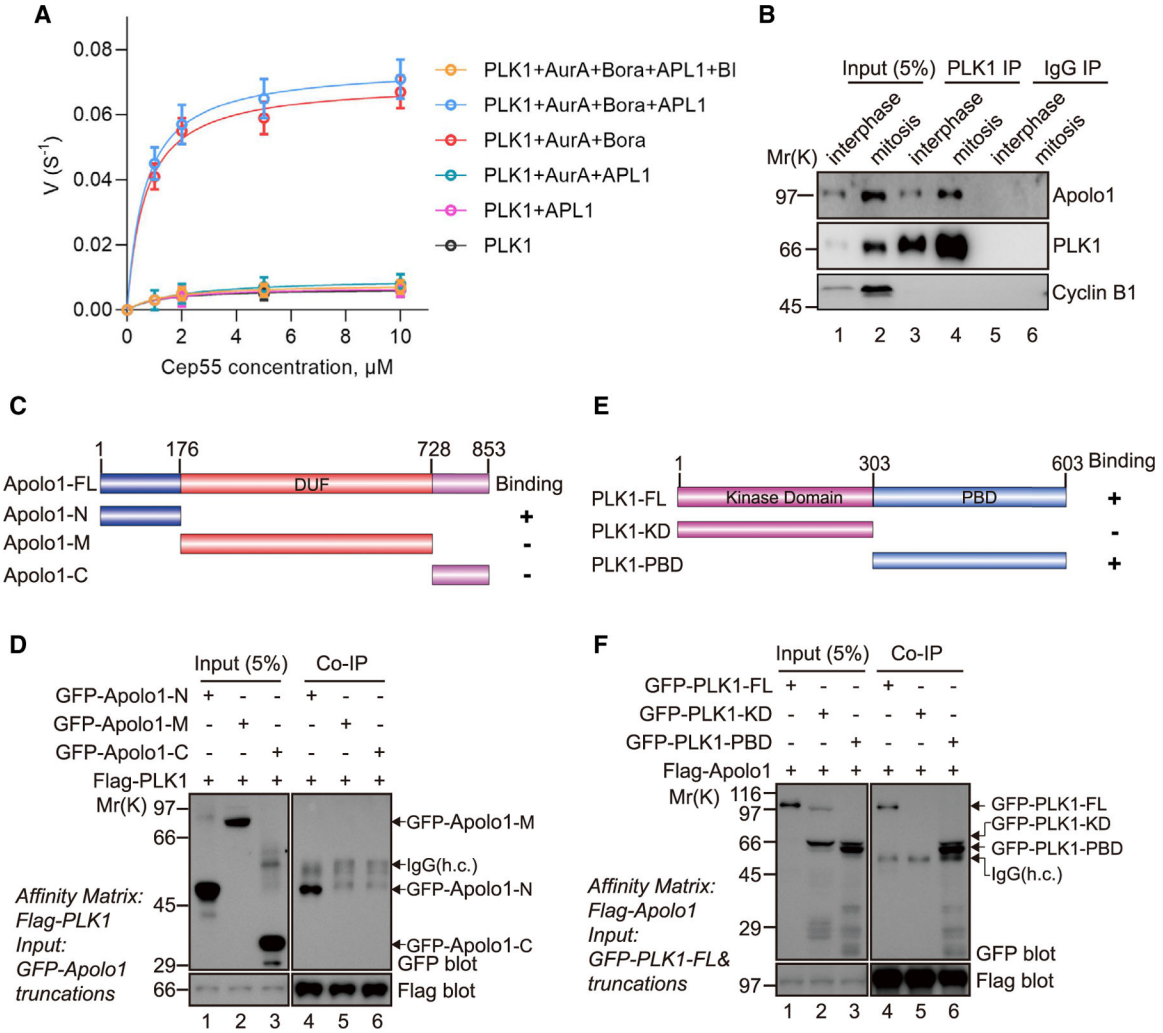

Figure 3. Apolo1 is a bona fide PLK1 regulator

(A) Kinase activity measurement of PLK1 in the presence of Apolo1, Bora, Aurora A, and their combination. Bacterially recombinant PLK1 exhibits no kinase activity and requires activation by Bora and Aurora A. An aliquot of BI2536 was included to determine minimal PLK1 kinase activity. Apolo1 alone did not activate PLK1 kinase activity.

(B) Endogenous PLK1 immunoprecipitates from interphase (2 mM thymidine, 16 h) and mitosis (100 ng/mL nocodazole, 16–18 h) HeLa cells were detected with antibodies against Apolo1, PLK1, and Cyclin B1.

(C) Schematic illustration of full-length and deletion mutants of Apolo1. Specifically, Apolo1-N indicates 1–176 aa, Apolo1-M indicates DUF (177–728 aa), and Apolo1-C indicates 729–853 aa.

(D) Coimmunoprecipitation assay of FLAG-PLK1 and GFP-Apolo1 truncation fragments in 293T cells.

(E) Schematic illustration of PLK1 full-length and domain regions. Specifically, PLK1-KD represents the PLK1 kinase domain (1–303 aa) and PLK1-PBD represents the PLK1 polo-box binding domain (304–603 aa).

(F) Coimmunoprecipitation assay of FLAG-Apolo1 with GFP-PLK1 full-length and truncation fragments in 293T cells.
See also Figures S2 and S3.

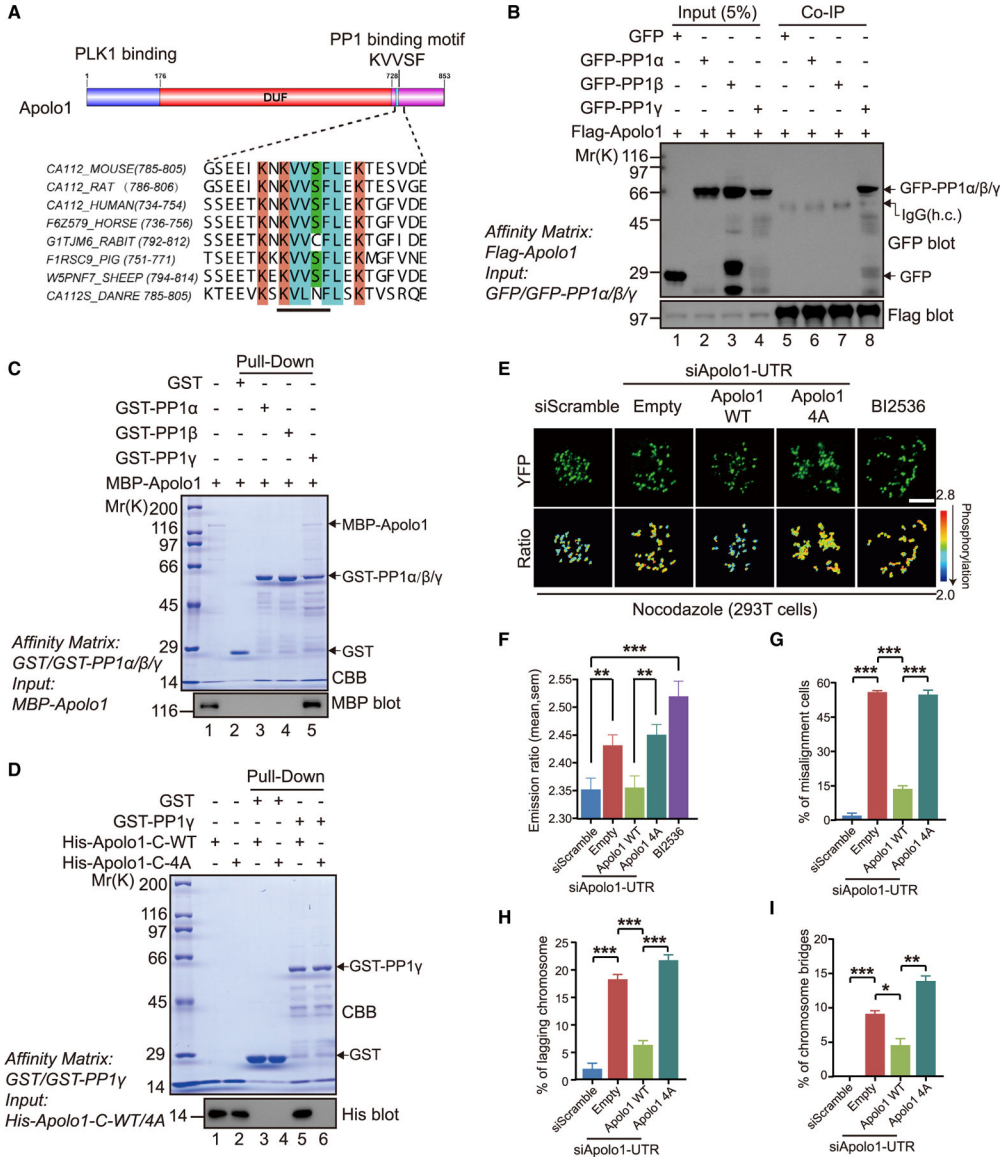

Figure 4. Apolo1 interacts with PP1γ directly via the canonical PP1 binding motif

(A) Apolo1 contains a conserved KVVSF motif responsible for PP1 binding (upper panel). Alignment of Apolo1 protein sequences in different species using the ClustalX algorithm (lower panel).

(B) Coimmunoprecipitation assay: FLAG-Apolo1 was cotransfected with GFP-PP1α/β/γ separately in 293T cells and analyzed by western blotting. Antibodies against to GFP and FLAG were detected.

(C) *In vitro* pull-down assay of GST-PP1α/β/γ with MBP-Apolo1 (full length). The gel was stained with Coomassie brilliant blue (CBB) (upper panel). Western blotting analysis with anti-MBP antibody (lower panel).

(D) *In vitro* pull-down assay of GST-PP1γ with His-Apolo1-C WT and 4A (KVVSF mutated to AVAAA). The gel was stained with CBB (upper panel). Western blotting analysis with anti-His antibody (lower panel).

(E) Control or Apolo1-depleted 293T cells were cotransfected with mCherry-Apolo1 WT or the 4A mutant, together with the Hec1-PLK1 sensor, and imaged at prometaphase. 293T cells were synchronized with 100 ng/mL nocodazole for 2 h after release from single thymidine treatment. BI2536 was added at 100 nM for 0.5 h. Scale bar, 5 μm.
(F) Statistical analyses of the FRET/CFP emission ratio as in (E). At least 20 cells of each group were counted. Data represent mean ± SEM from three independent experiments. Statistical significance was tested by two-sided t test and represented by asterisks corresponding to $^{**}p < 0.01$ and $^{***}p < 0.001$.
(G–I) Representative mitotic phenotypes in HeLa cells transfected with siScramble or siApolo1 (3′ UTR) only or cotransfecting siApolo1 (3′ UTR), together with FLAG-Apolo1 WT or 4A mutant plasmids, shown by time-lapse imaging and visualized with Hoechst-33342 staining (red arrowheads indicate chromosome misalignments, lagging chromosomes, or chromosome bridges). Quantification of chromosome segregation defects of live HeLa cells (siScramble, n = 97; siApolo1-UTR, n = 120; siApolo1-UTR+Apolo1-WT, n = 109; siApolo1-UTR+Apolo1–4A, n = 115). Cells exhibiting unaligned chromosomes and failing to align at the metaphase plate within 60 min after NEBD were considered misalignments. Data represent mean ± SEM from three independent experiments. Statistical significance was tested by two-sided t test; $^{**}p < 0.01$, $^{***}p < 0.001$.
See also Figure S4.

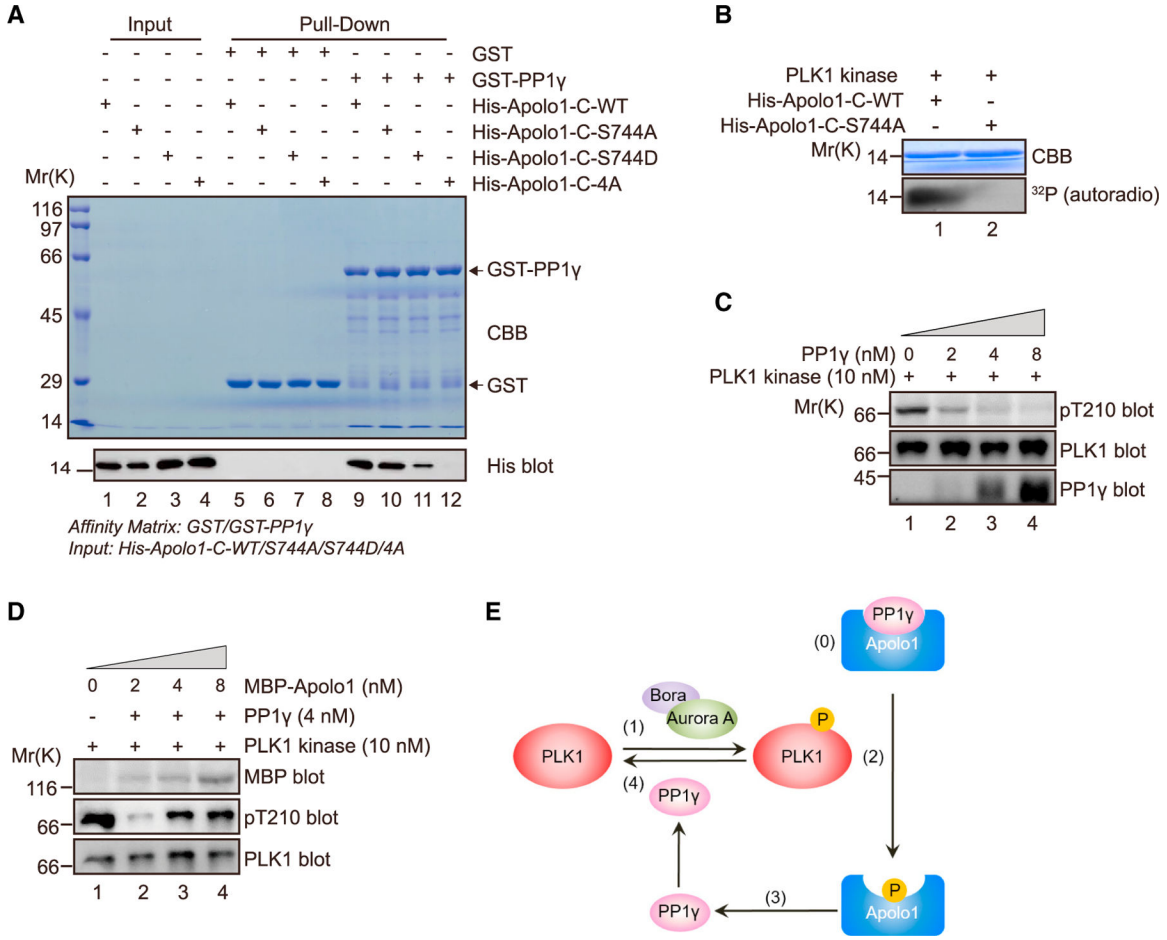

Figure 5. PLK1-Apolo1-PP1γ interactions constitute a feedback loop to orchestrate PLK1 activity in mitosis

(A) *In vitro* pull-down assay using GST-PP1γ as the affinity matrix to isolate His-Apolo1-C recombinant proteins (WT/S744A/S744D/4A). The gel was stained with CBB (upper panel). Western blotting analysis with anti-His antibody to annotate His-Apolo1-C proteins (lower panel).

(B) *In vitro* kinase assays using the PLK1 kinase to phosphorylate His-Apolo1-C WT and S744A mutants. CBB staining of purified proteins and an autoradiogram showing incorporation of radioactive γ−^{32}P ATP. PLK1 failed to phosphorylate the S744A mutant (lane 2).

(C) *In vitro* phosphatase assay using purified PP1γ phosphatase and active His-PLK1 kinase as substrate. Purified active PLK1 kinase from insect cells was incubated without or with increasing concentrations (at indicated concentrations) of PP1γ phosphatase. Phosphorylation of PLK1 pT210 was detected by phospho-specific antibodies (pT210-PLK1). Equal loading was monitored by PLK1 blotting.

(D) *In vitro* phosphatase assay was performed as described in (C). Active PLK1 kinase was incubated with PP1γ phosphatase and gradient MBP-Apolo1 (at indicated concentrations). Phosphorylation of PLK1 at Thr210 was detected by pT210-PLK1 antibody. Equal loading is evident through PLK1 blotting.

(E) Working model for the PLK1-Apolo1-PP1γ feedback loop in mitosis. Apolo1 binds to PLK1 at kinetochores during prometaphase and protects PLK1 from PP1γ-elicited dephosphorylation by sequestering PP1γ. As Apolo1 is phosphorylated by PLK1 at the kinetochores, PP1γ is released from Apolo1. PP1γ then dephosphorylates PLK1 to reduce PLK1 activity.

See also Figure S5.